Environmental Performance Bounds for Undersea Pulsed Laser Serial Imagers

Fraser R. Dalgleish, Anni K. Vuorenkoski, Gero Nootz, Bing Ouyang and Frank M. Caimi

Harbor Branch Oceanographic Institute at Florida Atlantic University
5600 US 1 North, Fort Pierce, FL, USA 34946
Tel. 772-242-2591 E-mail fdalglei@hboi.fau.edu

ABSTRACT

This paper examines imaging performance bounds for undersea electro-optic identification (EOID) sensors that use pulsed-laser line scanners to form serial images, typically utilizing one laser pulse for each formed image element. The experimental results presented include the use of two distinct imaging geometries; firstly where the laser source and single element optical detector are nearly co-aligned (near monostatic) and secondly where the laser source is deployed on a separate platform positioned closer to the target (bistatic) with the detector being positioned much further from the target. The former system uses synchronous scanning in order to significantly limit the required instantaneous angular acceptance function of the detector and has the desired intention of acquiring only ballistic photons and the undesirable property of acquiring multiply-scattered snake photon contributions that indirectly arrive into the detector aperture. The latter system utilizes a staring detector with a much wider angular acceptance function, the objective being to deliver maximum photon density to each target element and acquire diffuse, snake and ballistic photon contributions in order to maximize the signal. The study investigates received pulse energy variance from both the direct (target) component and the snake (forward scatter) in clear filtered water, as well as various well-characterized particle suspensions with and without an artificial thin random scattering layer. For each dataset, efforts were made to measure variance due to device shot noise in order to assess the impact of the environment on image quality.

I. INTRODUCTION

There are a variety of scientific, homeland security, and defense applications for compact *in situ* electro-optic sensors which are effective in identifying and classifying natural and man-made objects in turbid underwater environments. Performance of existing underwater electro-optics sensors is well understood from development of accurate radiative transfer performance prediction models and experimental results obtained in highly controlled testing environments.

Several varieties of underwater electro-optic imaging sensors are currently used, each of which has been engineered to reduce the main mechanisms responsible for loss in image quality due to scattering and attenuation. Laser Line Scan (LLS) underwater imaging is a serial imaging technique which involves the optical scanning of a narrow instantaneous field of view (IFOV) receiver in a synchronous fashion with a highly collimated laser source over a wide swath of seabed. It is widely regarded as the optimal technology for extended range underwater optical imaging, with up to 6 attenuation lengths achievable in turbid sea water [1][2][3][4]. These imagers, which typically utilize moderate-power green continuous wave (CW) lasers, require an adequate laser-receiver separation to reduce the imaging detriment of near-field multiple backscatter. Currently available systems are large and require too much power to make them suitable for modern unmanned underwater platforms such as the man-portable autonomous underwater vehicle (AUV). For compact implementations of CW-LLS, the detection of target signals becomes obstructed by temporal overlap from volume scatter in turbid water, as well as loss of dynamic range due to ambient light. To increase their operational range and provide high quality identification-quality imagery, detection methods must be capable of separating the target and volume scattering signals to estimate the energy returning from the target alone. As the system approaches a contrast or power limit, over-sampling techniques, which average many samples for each image pixel, can be used to increase signal to noise ratio and hence improve image contrast, albeit with a reduction of image resolution due to intra-pixel scan and platform motion. Because effective pixel dwell times can be as long as 100μs, it is believed that CW LLS systems are more

robust to scattering inhomogeneities than the pulsed LLS, which can have effective pixel dwell times of only a few nanoseconds.

Another maturing technique used for extended range underwater imaging systems is range-gating, where the source and receiver are temporally synchronized using a pulsed laser, gated or time discriminating array detector, and knowledge of the time of arrival of the target signal. These methods also have the potential to determine precise distance from the travel time of the light pulses, and from a system packaging perspective, pulsed-gated imager architectures are amenable to a more compact implementation with reduced possible laser-receiver separation. Such techniques can allow separation of the target and scattering volume return signals, thereby increasing the imaging range under certain conditions. Several previous configurations using spatially broadened laser pulses and precisely gated, intensified cameras were built and tested, with results indicating imaging performance beyond 6 beam attenuation lengths [4][6][7][8][9][10]. However, employing wide-angle array detectors, the systems are photon inefficient and very susceptible to image degradation due to multiple forward scatter in very turbid water, even when extremely short gate times are used. Furthermore these systems don't offer the wide swath (~70 degrees) imagery which LLS systems can provide.

Recent work has focused on investigating time-resolved pulsed LLS techniques, both in simulation [5] and experimentally [11]. A pulsed near monostatic LLS radiative transfer model was developed [12] by Metron (Reston, VA) that allows the user to configure the medium with depth dependant inherent optical properties (IOPs) and recent studies have been conducted into the effect of thin scattering layers on image quality, known as the 'Shower Curtain Effect' [13]; however evaluation of the impact of randomly varying scattering layers on image quality is not possible with these models to date.

Current research also investigates distributed-LLS concepts, which are somewhat unconventional because the imaging system's components (scanned illuminator and staring receiver) are distributed among multiple platforms. For the purpose of this paper, this type of imaging architecture is known as the 'bistatic' geometry.

Originally demonstrated as a diver-deployed technique in the 1970s [17], this approach has been shown in recent test tank trials to offer a vast range and image quality improvements over single-platform techniques [14] [15] [16], and test tank demonstrated using a communication technique to implement a multistatic configuration [18]. A Monte Carlo time-resolved radiative transfer model is currently under development by Metron for these more flexibly deployed imaging and non line of sight (NLOS) communications architectures.

The experiments described in this paper therefore had the specific objectives of examining the impact of small temporal and spatial scale inhomogeneities in the seawater medium on the imaging performance of one-pulse-per-pixel serial underwater imagers. In natural waters these inhomogeneities can be attributed to zooplankton, large mineral particles, aggregates, biological scattering layers or turbulence. Previous efforts have focused on investigating performance of CW and pulsed serial imaging techniques in near monostatic geometries, examining degradation due to attenuation, volumetric scatter and forward scatter blur in approximately homogenous scattering suspensions using a high spatial frequency target. Image noise levels for the benchtop pulsed-LLS demonstration [12] were significantly influenced by laser energy jitter (>20%), due to limitations with available laser technology, the effect of which was far more significant in clear water. Normalization on a pulse-to-pulse basis using a reference detector is non-trivial and complicates system design. For the experiments described in this paper a more stable pulsed laser source (< 3% energy jitter) was used, but a another objective of the work was to determine what level of laser source pulse energy variance is acceptable for these classes of electo-optic imager. Also of particular interest was to assess the image noise contribution due to the forward scattering component, as it has been found in previous studies [12] that the pulsed LLS imager is limited by forward scatter noise. The main effect of forward scattering is a blurring of the image, but more knowledge of the variance of that signal component is desirable. Perhaps primarily, the motivation to perform the experiments described herein, was to capture important effects that radiative

transfer models cannot currently predict in order to understand limiting factors to allow for better system design of future systems.

II. BACKGROUND

In order to understand the potential for turbid water imaging performance improvement with the pulsed serial imaging alternatives, it is necessary to examine the light propagation process and interactions between the photons, the environment, the target and the optical receiver.

Near-Monostatic LLS

The objective of the near monostatic LLS architecture is to maximize photon density on each target element, suppress unwanted backscattered and forward-scattered light, but still collect the image-bearing photons returning from the target element. It accomplishes this by employing a synchronously-scanned collimated laser beam and narrow receiver field of view in a near monostatic configuration. For the results presented in this paper the separation between the laser source and receiver was 23 cm. Figure 1 shows the general LLS imaging geometry at a single instant during a line scan. It can be seen that many possible paths exist for both direct and scattered light to follow from being emitted from the laser source, to eventually returning to the receiver to form a pixel of the image.

Light which doesn't make it as far as the target, but is still gathered by the receiver is known as backscatter. As shown in figure 1, backscatter can be further categorized into light which either takes a multiply scattered 'shortcut' to the receiver or light which is initially scattered in the common volume formed between the laser source and the instantaneous field of view (IFOV) of the receiver. Figure 1 (left) illustrates this phenomena from normalized measured pulse time history plots for both clear water (dark line) and water with high particle concentration (lighter line). The first broad return is due to multiple scattering from particles near the receiver, where the laser energy is greatest. This is followed by the narrower return from common volume

backscatter, defined by the intersection of the receiver field-of-view with the laser beam. Finally, the reflection from the target in the object plane arrives at the receiver. The common volume backscatter peak occurs close to the onset of the common volume region since the intensity of the laser pulse falls off exponentially as it transits the common volume. At higher turbidities, the multiple backscatter return is significant and overlaps the common volume backscatter return.

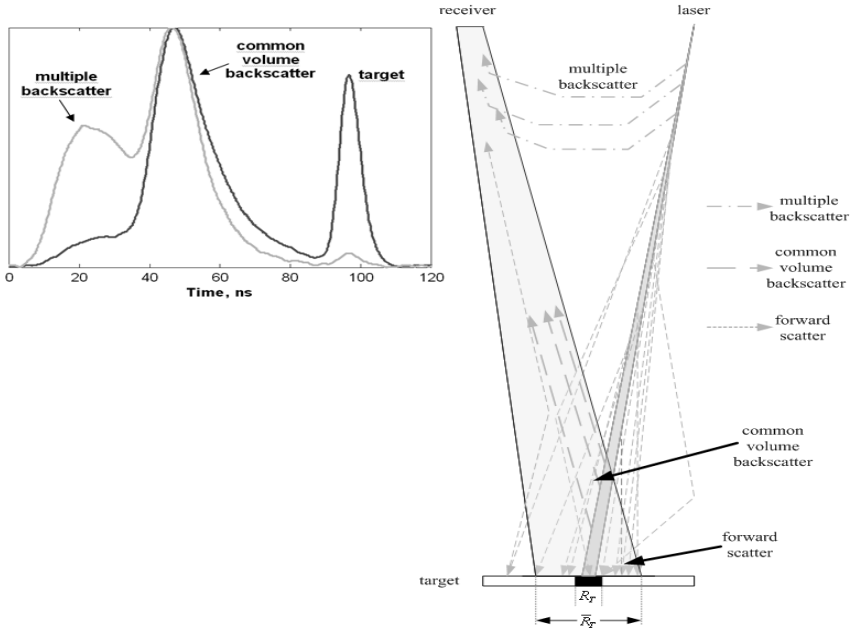

Figure 1. Near monostatic LLS imaging geometry at a single instant during a line scan, showing possible routes into the receiver aperture for defined categories of scattered and direct light. Representative normalized laser pulse time-history measurements for two turbidities are also shown. At the higher turbidity (lighter line) the multiple backscatter peak is stronger and the target return is weaker.

The effect of backscatter on an acquired image is a reduction in contrast and signal to noise ratio. Backscatter is independent of target reflectance and can be reduced by increasing the source-receiver separation, or decreasing the laser and receiver angular apertures. However, as the scattering particle concentration increases, multiple-scattered backscatter levels increase, eventually leading to the contrast limit for a CW LLS system. The time-resolved pulsed LLS allows for removal of the backscatter component using electronic or digital gating.

Not all the light received by a LLS system that has been reflected from the target contains useful information about the region of target being scanned at that instant in time. The component of the received light which has made it to the target, but which has undergone scattering with particles on the outgoing path is known as the forward scattered component. Carrying reflectance information from a larger region of the target $\bar{R}_T$ (shown in figure 1) the main effect of forward scatter on an acquired image is a reduction in resolution, contrast and signal to noise ratio, particularly when the surrounding target has a high mean reflectance and forward scatter appears as a blurring or glow. For the non-coherent, direct detection LLS systems being discussed in this paper, one possible approach to minimize forward scatter is to reduce laser and receiver angular apertures, but such a scheme leads to the system becoming photon deficient in turbid water. Another possible approach would be to reduce the path length from the laser to the target, *a la* bistatic LLS.

The image component that contains useful reflectance information from the small region of the target R_T (shown in figure 1), which is illuminated by the unscattered laser beam, is called the direct component. This consists of light which has not been scattered out of the main beam on the way to the target, but can consist of light which has undergone multiple small angle scattering on the way back from the target to the receiver, through those combinations of angles that allow acceptance into the receiver aperture. Allowing for temporal removal of the backscatter component, each pixel formed by the near monostatic pulsed LLS imager consists of the linear superposition of only the direct and forward-scattered components of returning light present at the receiver.

Bistatic LLS

In order to better understand the bistatic LLS technique, it is necessary to examine the light collection process in a turbid water environment. As is the case with all extended range underwater imaging architectures, the objective is to maximize photon density on each target element, suppress unwanted volumetric scatter and forward scatter while still collecting the image-bearing photons returning from the target. The bistatic LLS

accomplishes this by exercising spatial and angular disparity between source and receiver. For the results presented in this paper the separation between the source and receiver was almost 12 m. Figure 2 shows the bistatic LLS imaging geometry at a single instant during a line scan. It can be seen that multiple paths exist for both direct and scattered light as it passes between the laser source to target, and from target to receiver. Once again, light which doesn't reach the target, yet is gathered by the receiver, is considered as volumetric backscatter. In this simplified analysis, any contribution from upwelling or scattered sunlight is not considered, but with wide angle detection receiver configurations, ambient light leakage is a major consideration for daylight operations in shallow coastal waters. This further motivates the use of pulsed laser sources and receiver designs with good out-of-band rejection.

Figure 2 also illustrates this phenomena from measured pulse time history plots for clearer water ($c=0.7m^{-1}$) and also water with high particle concentration ($c=2.5m^{-1}$). In the more turbid case, the first return at the receiver is due to multiple scattering from the common volume and is overlapped by the delayed reflection from target. Multiple scatter also dominates on the return path from the target resulting in the observable 20ns (4.5 m) tail on the target return. The volume scatter is subject to time delay for the same reason, resulting in volumetric scatter being mixed with the target signal and the forward scatter signal.

At higher scattering coefficients almost all image bearing photons have been scattered multiple times before reaching the receiver. For the bistatic configuration, temporal separation of the overlapping direct, backscatter an forward scatter signal contributions is not possible, instead the choice of geometry reduces the undesirable signal levels.

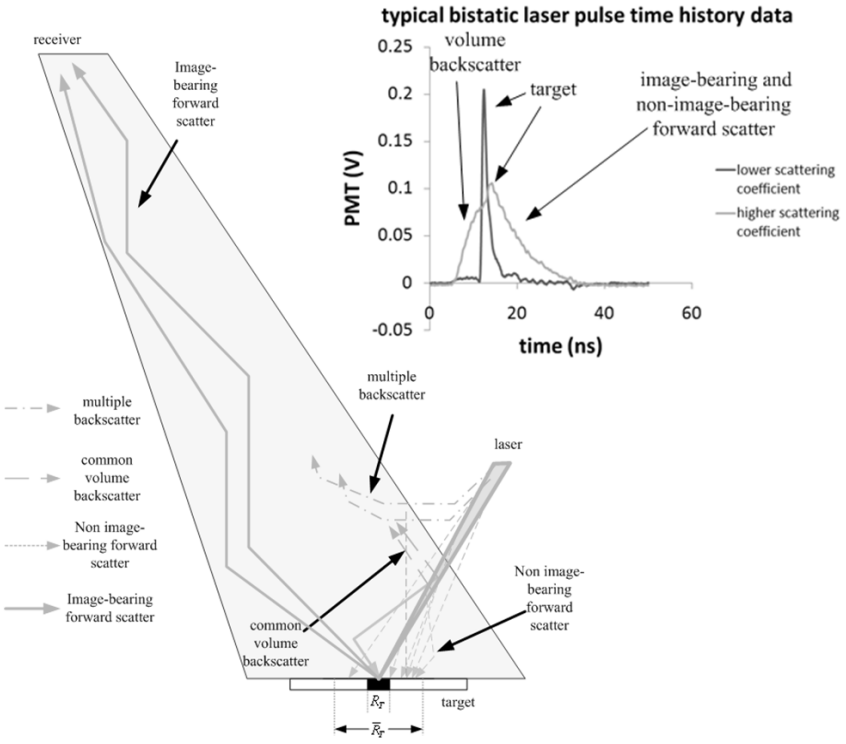

Figure 2. Bistatic LLS imaging geometry at a single instant during a line scan, showing possible routes into the receiver aperture for defined categories of scattered and direct light. A typical bistatic LLS laser pulse time history is also shown for clear water and more turbid water. Source-to-target distance = 2m; target-to-receiver distance = 10.75m.

A noticeable attribute of the bistatic imaging geometry in previous turbid water tests [15] was the robustness of image performance in non line of sight (NLOS) geometries, meaning that when there was no direct path between the target and the receiver, image reception was seen to be possible through a wide range of receiver pointing angles; this has potential advantages in flexibly deploying a system without needing to track transmitter position precisely. For this reason, during the tests described herein, it was also of interest to investigate pulse-to-pulse variance of the target signal in NLOS geometries.

III. EXPERIMENTAL CONFIGURATION

For both imaging geometries considered, experiments were conducted within the main test tank at the Ocean Visibility and Optics Laboratory at Harbor Branch Oceanographic Institute (Fort Pierce, FL), a campus of Florida Atlantic University. These tests consisted of acquiring many single pulse measurements using a large

(1.3 m x 1.3 m) static uniform reflectance (estimated reflectance of 70%) test target at realistic stand-off distances (for near monostatic tests, the stand-off distance was 10 meters; for bistatic tests the laser to target distance was 1.8 meters and the target to receiver distance was 11 meters) in the alternate geometries (see figure 6) through a range of carefully controlled particle suspensions. A 40 μJ 532nm pulsed laser with 500 ps pulse duration, 500 Hz repetition rate and near diffraction limited beam quality was used for both sets of experiments.

A linear bubble generator was also placed in the tank to provide a simple way to create a random, albeit uncharacterized, scattering inhomogeneity into the test volume (see figure 3).

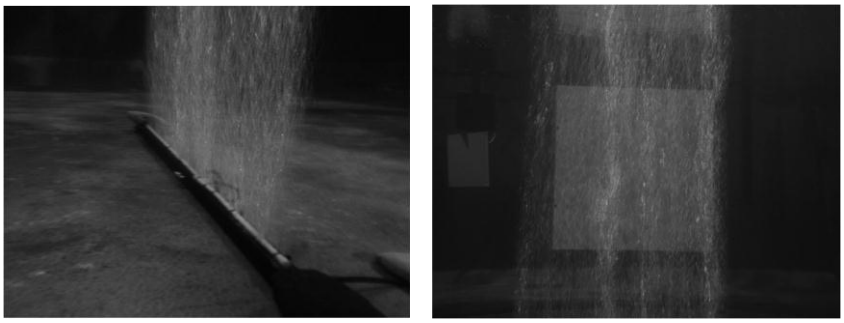

Figure 3. Bubble screen in test tank to create a random thin scattering layer

An experiment was conducted to measure the attenuation characteristics of the bubble curtain. The attenuation coefficient was measured with LISST-Stokes (Sequoia Scientific, Bellevue, WA), a diffraction based laser scattering meter. The transmission measurement of the instrument indicated the attenuation coefficient was between 0.5 and 1.0 m^{-1} at 532nm.

Ultra-fine Arizona test dust was used to increase the beam attenuation coefficient (c) values from clear water up to c=0.939 m^{-1} at 532nm (i.e. almost 10 beam attenuation lengths) in several increments for the near monostatic tests. For the bistatic tests, c values from clear water up to c=3.13 m^{-1} were produced (i.e. over 30 beam attenuation lengths). Optical properties were monitored by a Wetlabs ac-9 meter with attenuation and absorption being adjusted for scattering error according to Zaneveld [19]. Single scattering albedo was found

to be ≈ 0.90 throughout. In addition to measuring beam attenuation and absorption at 532nm, the forward portion (out to 7°) of the scattering phase function for the ultra-fine Arizona test dust was measured using the LISST-Stokes. The results are being used in ongoing Monte Carlo simulations of the scenarios.

A microchannel plate (MCP) photomultipler tube (PMT) (Hamamatsu R5916U-50) was radiometrically calibrated and measured for both impulse response and angular response function for each configuration. A 50mm diameter plano-convex lens with 100mm focal length was placed in front of the MCP-PMT. For the near-monostatic configuration a 1.5mm iris was also placed at the focal point to reduce the IFOV. The MCP-PMT was placed a short distance behind the iris to ensure that 60% of the 8mm active area was being flooded with the defocused light bundle. For the bistatic configuration, the iris was removed. Raytrace modeling results and experimental measurements of the IFOV for both configurations were in agreement that the IFOV was 15 milliradians (< 1 degree) full angle for the near monostatic experiments and 150 milliradians (< 10 degrees) for the bistatic configuration (no iris) both with a flat top angular response.

The range of linearity of the MCP-PMT device was determined experimentally using a variable beam expander and set of calibrated neutral density filters by flooding the photocathode and measuring the peak output current to known input irradiance. This was necessary to establish the linear range of output current from the device during the experiments and also to determine the conversion factor between input peak power and measured output peak voltage. The impulse response of the device was measured at less than 900 ps, which was deemed sufficiently fast to faithfully record an undispersed laser pulse source waveform.

A reference signal was captured using a fast (9 GHz) photodiode detector (EOT-4000) and recorded at 10 GSps. The plot in figure 4 represents multiple consecutive pulses overlaid with standard deviation as a percentage of mean for both the integrated pulse energy and the peak value. Neglecting discretization error, this analysis established that the laser source was stable in energy to less than 3 %. The MCP-PMT was calibrated and characterized for pulse variance in a series of in air measurements (figure 5).

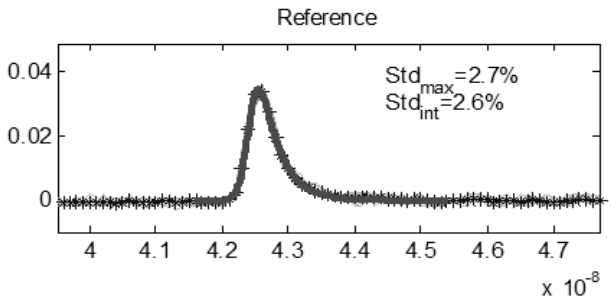

Figure 4. Multiple overlaid reference detector signal scope traces (showing < 3% calculated energy variation).

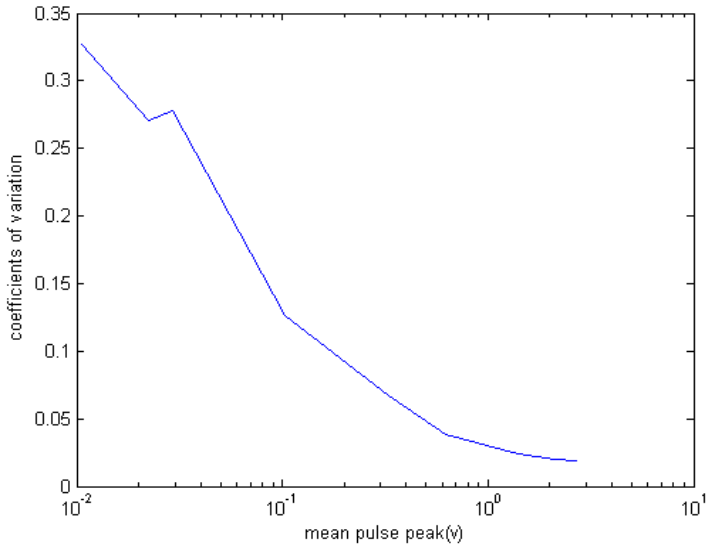

Figure 5. MCP-PMT device noise v.s. output voltage.

Near Monostatic Experimental Configuration

For the near monostatic tests, the laser and receiver were held stationary throughout. Two sets of experiments were conducted in this configuration. In a first forward scattering performance study, a 1.3m x 1.3m target panel was mounted 10 meters from the optical viewport on a linear drive stage for precise positioning (<0.5mm repeatability). A hole was drilled in the center of the target panel (2.54cm diameter). The target was moved perpendicular to the center of the imager optical axis between two positions, such that in one position the laser beam passed through the hole (determined in clear water) and in another position (20cm offset) the laser beam was reflected from the solid target panel.

The bubble line (figure 3) was placed 2 meters in front of the target. At each turbidity, with and without bubbles, 40 single pulse references, as well as recorded time history returns from the tank, were sampled at 10 Gsps on a 2.5 GHz bandwidth oscilloscope under control of a LabVIEW program. Figure 6 shows a schematic of the experimental configuration.

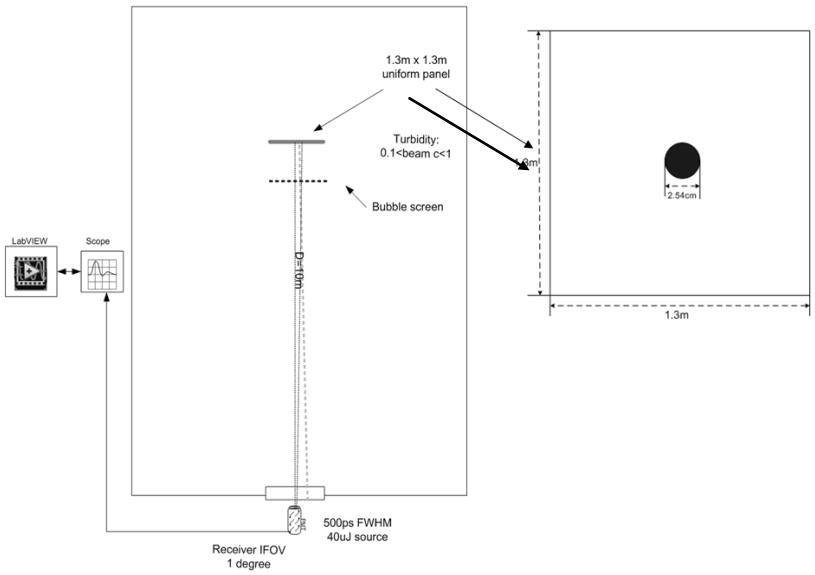

Figure 6. Plan view schematic of HBOI large optical imaging test tank configured for near-monostatic tests.

In the second experiment, a 20 cm x 30 cm target (Figure 7) replaced the panel used in the first experiment to conduct a imaging experiment. The target moved at 1 cm interval vertically and horizontally, at each position, 20 references and return from tank were recorded. At the lowest turbidity (c=0.085), data were also taken with the bubble screen in place. Data were recorded at 5 different turbidities (C=0.085, 0.389, 0.625, 0.825 and 1.02).

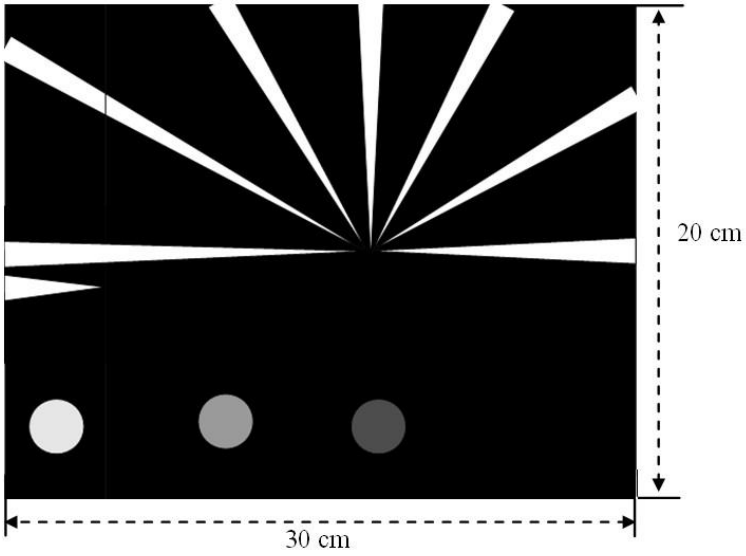

Figure 7. Imaging target used in Pulsed Imaging Experiment.

Bistatic Experimental Configuration

For the bistatic tests, the laser and same target panel were held stationary throughout. The receiver was mounted on a microstepper actuator stage and automatically rotated through a total angle of 68 degrees (-34 to +34 degrees about the LOS position) in 2 degree increments, acquiring 250 single pulse reference and time history datasets at each angular increment, turbidity, and with and without bubbles. The bubble screen (figure 3) was also placed 2 meters away from the target in the direction of the receiver. Figure 8 shows a schematic of the experimental configuration.

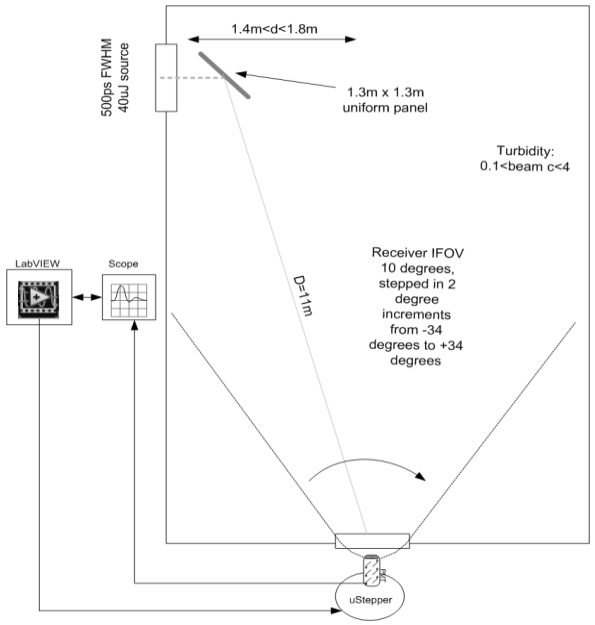

Figure 8. Plan view schematic of HBOI large optical imaging test tank configured for bistatic tests.

IV. RESULTS

In the near monostatic geometry, nine turbidity increments were produced. In an effort to control detector shot noise, which is proportional to the number of received photons, neutral density (ND) filters were used to limit the target signal photon flux and resulting peak current at the receiver for the clearer water cases. The MCP-PMT gain was held constant throughout. Figure 9 shows the mean signal at each turbidity for the non-bubble case. It can be seen that the target signal was held approximately constant by the removal of ND filters from clear water to $c=0.523m^{-1}$ (more than five attenuation lengths), beyond which no more filters are present and the target signal became greatly attenuated, eventually reaching a shot noise and power limited scenario at $c=0.939m^{-1}$. The data, however does allow evaluation of environmental noise through most of the operational envelope for this type of sensor (i.e. up to 5 attenuation lengths).

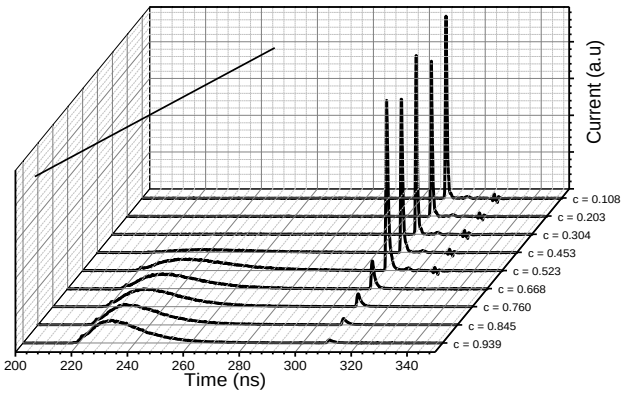

Figure 9. Summary of near monostatic experiments showing mean PMT signals for each turbidity without adjusting for ND filter values.

Coefficient of Variation (CV), the ratio between the standard deviation σ and mean m: $CV = \sigma / |m|$, were used when studying the noise statistics using the experimental data. Here the mean m is the average of the peaks of the target reflection of the multiple pulses recorded, and σ is the standard deviation of these peaks. In low turbidity experimental data, the peaks of each of the individual pulses were extracted directly. The location of the peaks were recorded to limit the search range when processing high turbidity data when the volume backscatter dominates the magnitude of the pulses.

Mean pulse peak m, overall pulse-to-pulse standard deviation $\sigma_{overall}$ were computed directly from the data to derive $CV_{overall}$: $CV_{overall} = \sigma_{overall} / |m|$. Under the assumption that the device noise and environment noise are statistically independent, the follow formula can be used to compute the standard deviation due to environmental noise using the PMT device noise statistics:

$$\sigma_{environment} = \sqrt{\sigma_{overall}^2 - \sigma_{device}^2} \qquad \textbf{Equation 1.}$$

where σ_{device} was computed via interpolation from the PMT device noise experimental data from the over the air experiment (Figure 5). Then CV due to environment: $CV_{environmen} = \sigma_{environmet} / |m|$ were then derived.

In the case that the laser was aimed at the solid part of the target panel, for the near monostatic architecture in homogeneous media (i.e. without bubbles) the CV from the target only (for the cases from clear water up to $c=0.523m^{-1}$) as a percentage of the mean was ≈ 10%, which is more than three times the reference pulse energy uncertainty, furthermore, the environmental noise dominates the overall noise. For the turbidities greater than $c=0.523m^{-1}$, the CV increases as signal photon flux decreases and the device noise started to dominates the overall noise (Figure 10(a)).

For the inhomogeneous media cases (i.e. with bubbles) the CV of the pulse energy from the target only (for the cases from clear water up to $c=0.523m^{-1}$) was ≈ 25%, which is more than six times the reference pulse energy uncertainty. For the turbidities greater than $c=0.523m^{-1}$, the noise also increases as signal photons decrease(Figure 10(b)). On the other hand, the contribution from environmental noise followed the same trend as in the homogeneous media case.

In the case that laser was pointed at the hole, it is interesting to notice that the strength of the target reflection actually increases with higher turbidity and reached the maximum at attenuation length = 4, before lost strength at even higher turbidity. The same phenomenon could be observed in both homogeneous and inhomogeneous media cases. This is due to the fact that in this scenario, there is no direct reflection from the target because of the hole, and at lower turbidity, the forward scattering strength is weak since most photons went through the hole. At increased turbidity, photons started to be spread to nearby target element and reflected back to the receiver, therefore resulted in increased reflect strength. However, eventually, further increase in turbidity led to less overall photons reaching the target and therefore reduced reflection strength. Regarding the noise distribution the same trend as in the case of solid panel still held.

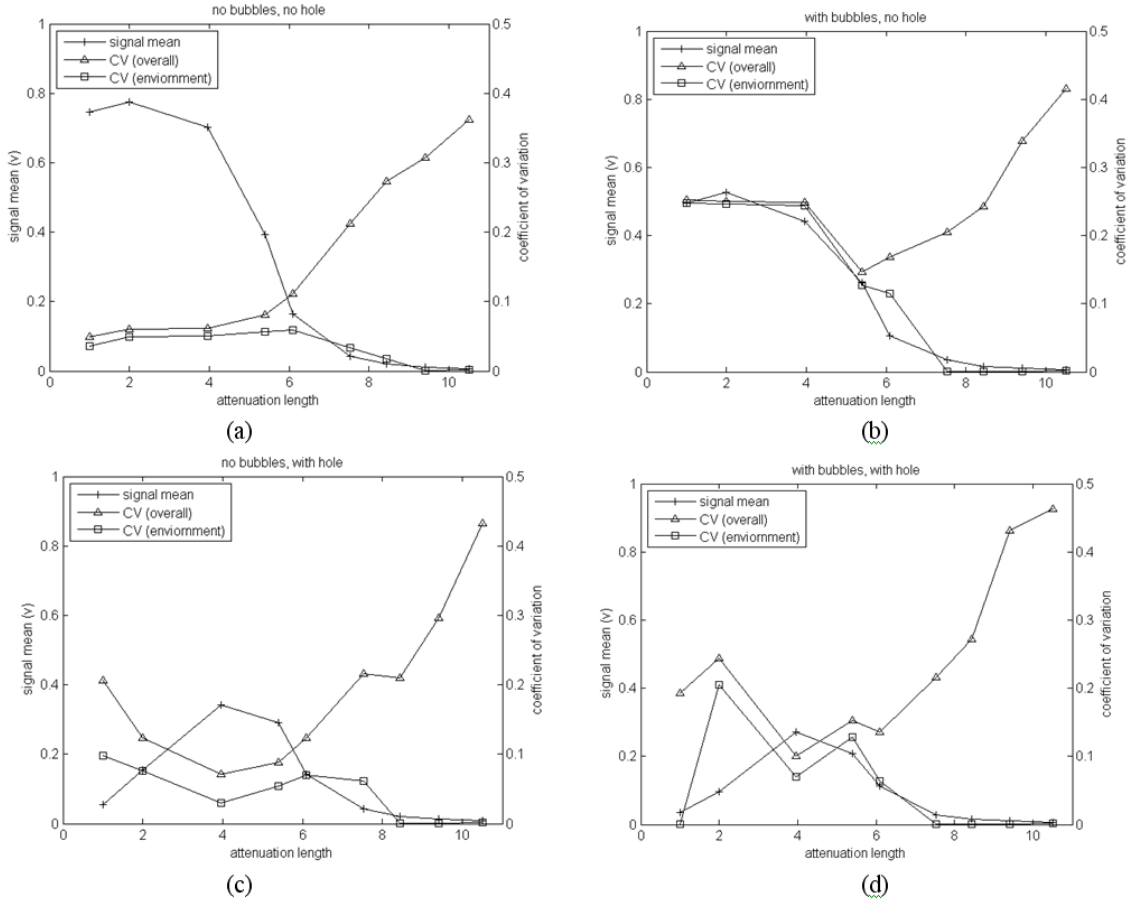

Figure 10. Integrated target return energy and standard deviation as a percentage of mean energy for monostatic case, with and without bubble curtain as a function of attenuation coefficient.

In the pulsed imaging experiment, the images were formed by extract the target peak from one single pulse at each location to form an image of 30x20 pixels. As mentioned above, the location of the target return at lower turbidity was recorded to be ensure correct peak to be extracted at higher turbidity when the volume scattering dominated. As shown in Figure 11 below, the image contrasts reduced with increased turbidity as expected, however was perceptible till attenuation length = 6.25.

Turbidity	CSNR	Images
0.83	10.1	
3.89	9.301	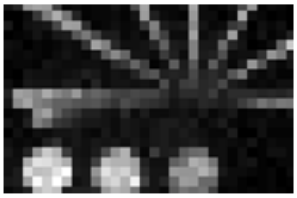
6.25	4.24	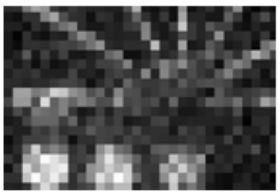
8.25	0.5143	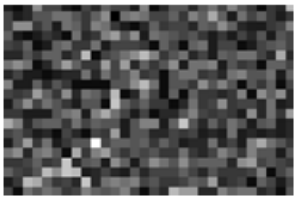
10.2	0.0239	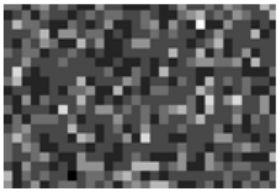

Figure 11. CSNR and images of near mono-static pulsed imaging at different turbidities

It is also interesting to examining the impact on images when the inhomogeneous layer presents in the media. As can be seen in figure 12 below, the inhomogeneous resulted in significant pixel variance, which is evident when examining the spectron at the lower left corner, this resulted in much lower CSNR number. However, it should also noted that the image sharpness is still maintained fairly well, and therefore still more visually pleasing than that at attenuation length = 6.25 even though the CSNR is lower (2.55 v.s. 4.24).

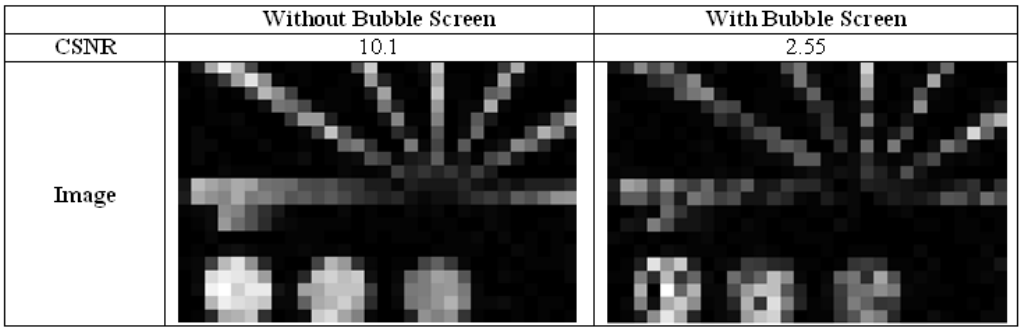

Figure 12. Comparison of CSNR and images of pulsed imaging with and without bubbles.

For the bistatic tests, the peak target signal in the center position was again manipulated with ND filters to be approximately constant for five of the eight turbidity steps from clear water up to c=2.04m^{-1}. In clearer water, as expected, the signal strength was very weak for the NLOS cases. It can also be seen from figure 13, which as the turbidity increases the return signal appears more constant over the angular range.

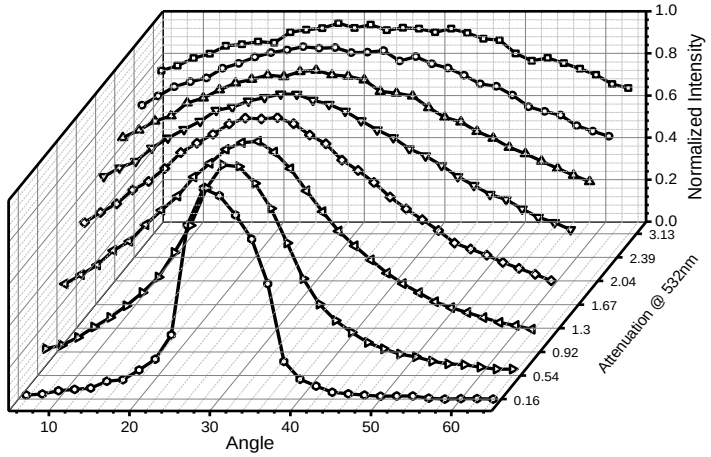

Figure 13. Summary of bistatic experiments showing normalized mean PMT signals for each turbidity as a function of angular offset for the non-bubble cases.

When the pulse energy statistics were analyzed for the bistatic cases, for clear water where the receiver was pointing directly at the target (LOS), they showed similar CV to the laser reference, but for NLOS and bubble curtain cases, they showed greatly increased CV (due to photon deficiency). However, through the entire range of turbidities, the CV was seen to remain at 3 % for the LOS case through c=2.39m^{-1}, gradually

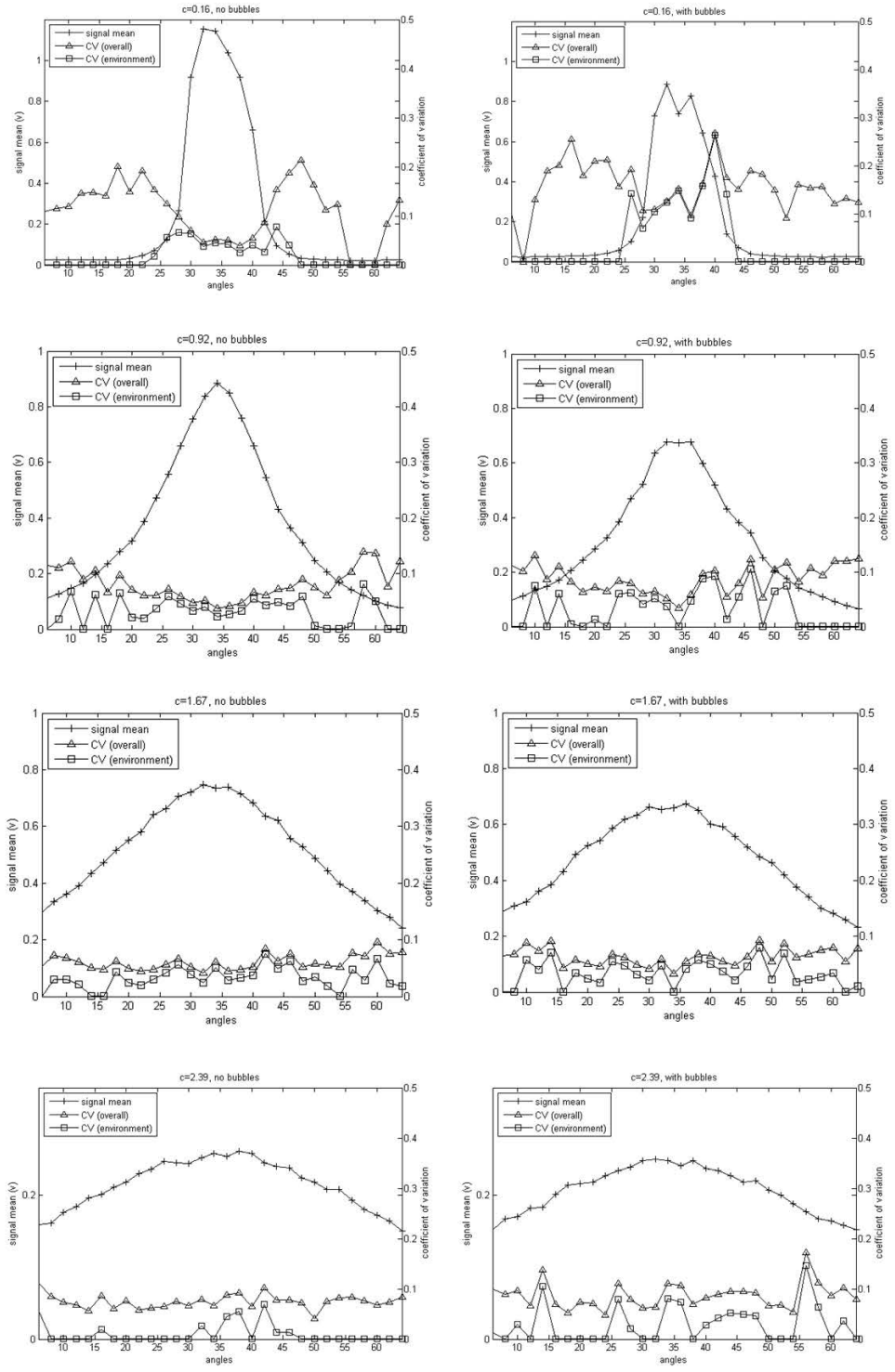

Figure 14. Bistatic geometry pulse statistics in clear water case and c=1.67m^{-1}, with and without bubbles.

spreading out over the NLOS cases with similarly low standard deviation. The effect of the bubble curtain also became less significant at increased turbidities. Figure 14 shows four different turbidities (attenuation length = 1.6, 9.2 16.7 and 23.9), with and without bubbles.

V. DISCUSSION

The results show that in the case of the near monostatic geometry, utilizing narrow angular source and receiver apertures combined with greater signal attenuation on the longer outgoing propagation path, imaging performance is more sensitive to random scattering inhomogeneities than in the case of the bistatic geometry. To obtain quality imagery from imaging systems that exhibit pixel-to-pixel intensity standard deviations of 10% or more will require raw images to be enhanced with processing methods such as deconvolution and other image processing techniques. Alternatively improvements in image quality could be achieved via system designs that use multiple pulses to allow temporal integration or coherent processing; and/or multiple detectors to spatially filter environmental and device noise at the image formation stage.

Multiple receiving systems (diversity receivers) have been used to improve the reliability of wireless communications systems for many years. In such systems, improvement of received signal quality is derived from the existence of multiple signal streams within the communications channel or medium. When signal coherence is maintained through the channel, multiple signals arriving at a single receiver via different paths are subject to fading through coherent combining due to relative time delays through each path. The net effect of using different receivers in the above scenario is to reduce the probability of error essentially by filling in deep fades with signals traveling different paths where destructive interference is less likely, resulting in a net gain—the so-called "diversity gain". It is therefore of interest to evaluate the potential of such improvement using a receiver consisting of multiple spatially diverged PMTs in an experimental underwater laser imaging/communication system. To that end, the bi-static experimental data were used to compare the CV of averaging of pulses recorded by PMT pointed to three different angles (28, 32 and 36

degrees) with that from one PMT at 32 degrees. As shown in Figure 15, averaging resulted in significant SNR improvement. This observation has inspired the development and deployment of a multiple PMT receiver (figure 16).

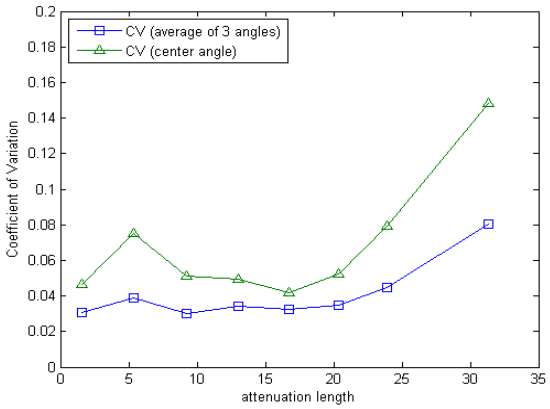

Figure 15. SNR improvement via averaging of pulses from multiple PMTs.

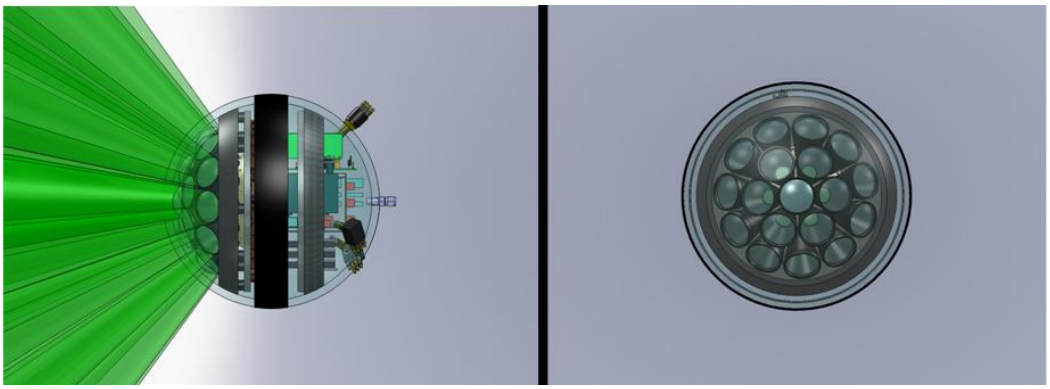

Figure 16. Multiple PMT Receiver for Underwater Laser Imaging/Communications

Follow-on to this work, would involve better characterization of the bubble curtain IOPs, development of accurate time-resolved radiative transfer code for the bistatic geometry and an accurate detector noise model, which are areas of ongoing research and development for the authors. Apparatus to allow at-sea testing and channel characterization with alternate configurations of pulsed-scanned laser imaging systems in a range natural conditions is currently being prepared.

VI. CONCLUSIONS

This work represents a practical contribution in the growing area of underwater pulsed serial imager system development. The main advantages of using pulsed scanned illumination are in delivering high photon flux to each target element to improve target signal detection in the highly attenuating and scattering environment of natural waters. For daylight systems, pulsed sources offer the possibility to isolate target signals despite DC biases resulting from the presence of ambient light leakage, in order to improve image contrast.

ACKNOWLEDGEMENTS

This work was conducted under a grant monitored by the US Office of Naval Research. This paper is Harbor Branch Oceanographic Institute's contribution number 1834.

REFERENCES

1. Strand, M.P., "Quantitative evaluation of environmental noise in underwater electro-optic imaging systems," Proc. Ocean Optics XIV, Kialua-Kona, HI, (1998).
2. Kulp, T.J., Garvis, D., Kennedy, R., Salmon, T. and Cooper, K. "Results of the final tank test of the LLNL/NAVSEA Synchronous-Scanning Underwater Laser Imaging System," Proc. Ocean Optics XI, Vol 1750, 453-464. (1992).
3. Gordon, A. "Turbid test results of the SM2000 laser line scan system and low light level underwater camera tests," Underwater Intervention ' 94: Man and Machine Underwater, Conference Proceedings, Marine Technology Society, 305-311, Washington D.C., (1994).
4. Strand, M.P., "Underwater electro-optical system for mine identification," Proc. SPIE 2496, 487-497 (1995).
5. Caimi. F. M. and Dalgleish, F. R., 2010, "Performance considerations for continuous-wave and pulsed laser line scan (LLS) imaging systems," Journal of the European Optical Society – Rapid Publications 5, 10020S, 2010.
6. McLean, E.A., Burris, H.R. and Strand, M.P. "Short-pulse range-gated optical imaging in turbid water," Appl. Opt. 34, 4343. (1995).
7. Swartz, B.A. "Diver and ROV Deployable Laser Range Gated Underwater Imaging Systems," Underwater Intervention '93 Conference Proceedings, New Orleans, Marine Technology Society and Association of Diving Contractors, (1993).
8. Witherspoon, N.H. and Holloway. J.H. "Feasibility testing of a range-gated laser-illuminated underwater imaging system," Proc. SPIE Int. Soc. Opt. Eng. 1302, 414 (1990).
9. Fournier, G. R. Bonnier, D. Forand, J. Luc and Pace, P. W. "Range-gated underwater laser imaging system," Opt. Eng. 32, 2185. (1993).

10. Busck, J. "Underwater 3-D optical imaging with a gated viewing laser radar," Opt. Eng. 44, 116001, (2005).
11. Dalgleish, F. R., Caimi, F. M., Britton, W. B. and Andren, C. F. “Improved LLS imaging performance in scattering-dominant waters”, Proc. SPIE 7317, p. 73170E, 2009.
12. Giddings, T. E. and Shirron, J. J. “Numerical simulation of the electro-optical imaging process in plane-stratified media”, Opt. Eng. 48 (12), p. 126001, 2009.
13. Giddings T. E. and Shirron, J. J. “The shower curtain effect and electro- optical imaging sensors”, Ocean Optics XX, Anchorage, AK, Sept. 2010.
14. Dalgleish, F. R., Caimi, F. M., Vuorenkoski, A. K., Britton, W. B. and Ramos, B. “Experiments in bistatic Laser Line Scan (LLS) underwater imaging”, Proc. Marine Technol. Soc./IEEE Oceans Conf., 2009. Paper 090710-001.
15. Ouyang, B., Dalgleish, F. R., Vuorenkoski, A. K., Britton, W. B., Ramos, B. and Metzger, B. “Visualization for Multi-static Underwater LLS System using Image Based Rendering,” Submitted to IEEE Oceanic Engineering, 2011.
16. Mullen, L. J., Laux, A., Conconour, B. and McBride, W. “Extended Range Underwater Imaging using a Time Varying Intensity (TVI) Approach”, Proc. Marine Technol. Soc./IEEE Oceans Conf., 2009. Paper 090611-005.
17. Duntley, S. Q., Austin, R. W., Ensminger, R. L., Petzold, T. J. and Smith, R. C. “Experimental TVI system report”, Visib. Lab. Tech. Rep., pp. 74–1, 1974.
18. Dalgleish F. R., Ramos, B., Britton, W. B., and Caimi F. M., “Multistatic distributed laser line scan underwater imaging architecture”, Ocean Optics XX. Anchorage, AK. Sept. 2010.
19. Zaneveld, J.R.V., Kitchen, J.C. and Moore, C. “The scattering error correction of reflecting-tube absorption meters.” Ocean Optics XII, Proc. SPIE, 2258: 44-55. 1994.